

AD-A104 943

HUGHES RESEARCH LABS MALIBU CA  
LOW-LOSS FIBER WAVEGUIDES. (U)  
SEP 81 J A HARRINGTON

F/G 9/1

N00014-79-C-0691

NL

UNCLASSIFIED

| OF |  
40A  
104 943

END  
DATE  
FILED  
10-81  
DTIC

AD A104943

LEVEL

12

# LOW-LOSS FIBER WAVEGUIDES

J. A. Harrington

Hughes Research Laboratories  
3011 Malibu Canyon Road  
Malibu, CA 90265

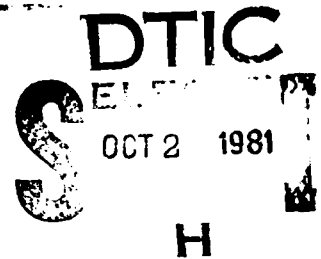
September 1981

N00014-79-C-0691

Annual Technical Report

1 August 1980 to 30 June 1981

*Approved for public release; distribution unlimited.*



Prepared for  
MATERIAL SCIENCES DIVISION  
Office of Naval Research  
800 North Quincy Street  
Arlington, VA 22217

DTIC FILE COPY

81 10 2 097

UNCLASSIFIED

SECURITY CLASSIFICATION OF THIS PAGE (When Data Entered)

REPORT DOCUMENTATION PAGE		READ INSTRUCTIONS BEFORE COMPLETING FORM
1. REPORT NUMBER (6)	2. GOVT ACCESSION NO. AD A104943	3. RECIPIENT'S CATALOG NUMBER
4. TITLE (and Subtitle) LOW-LOSS FIBER WAVEGUIDES	9	5. TYPE OF REPORT & PERIOD COVERED Annual Technical Report 1 Aug 80 - 31 Jun 81
7. AUTHOR(s) J.A. Harrington	15	6. PERFORMING ORG. ORGANIZATION NUMBER
9. PERFORMING ORGANIZATION NAME AND ADDRESS Hughes Research Laboratories 3011 Malibu Canyon Road Malibu, California 90265	10. PROGRAM ELEMENT, PROJECT, TASK AREA & WORK UNIT NUMBERS	
11. CONTROLLING OFFICE NAME AND ADDRESS Material Sciences Division Office of Naval Research 800 No. Quincy St., Arlington, VA 22217	12. REPORT DATE Sep 1 1981	
14. MONITORING AGENCY NAME & ADDRESS (if different from Controlling Office)	13. NUMBER OF PAGES 57	
16. DISTRIBUTION STATEMENT (of this Report)	15. SECURITY CLASS. (of this report) UNCLASSIFIED	
	15a. DECLASSIFICATION/DOWNGRADING SCHEDULE	
17. DISTRIBUTION STATEMENT (of the abstract entered in Block 20, if different from Report)	S H	
18. SUPPLEMENTARY NOTES	DTIC ELECTED OCT 2 1981 D	
19. KEY WORDS (Continue on reverse side if necessary and identify by block number) Infrared fibers, optical materials, fiber optics, light scattering, crystal growth.	7	
20. ABSTRACT (Continue on reverse side if necessary and identify by block number) This annual report summarizes our second year of effort to fabricate low-loss fiber waveguides with potential loss near $10^{-3}$ dB/km. To develop such low-loss waveguides, we have used alkali and thallium halides to form poly- and single-crystal fibers. To date our best poly-crystalline KRS-5 (TlBrI) fiber remains 5 orders of magnitude above the goal of $10^{-3}$ dB/km.		

DD FORM 1 JAN 73 1473 EDITION OF 1 NOV 65 IS OBSOLETE

UNCLASSIFIED

SECURITY CLASSIFICATION OF THIS PAGE (When Data Entered)

172600

UNCLASSIFIED

SECURITY CLASSIFICATION OF THIS PAGE When Data Entered

Our approach to developing low-loss waveguides involves three interrelated tasks: (1) fiber materials preparation, (2) fiber fabrication, and (3) optical evaluation and analysis. In the first task, we have combined our reactive atmosphere process (RAP) chemistry techniques, which have proven so successful for alkali halides and zone refining; to prepare thallium halide crystals for use in fiber fabrication. While we have yet to evaluate these crystals optically, we expect substantial reduction in the anion impurity concentration.

In the second task, we devoted the majority of our efforts to the fabrication of SC fibers. The fabrication of SC fibers holds, we feel, the greatest promise for achieving the program goal of  $10^{-3}$  dB/km. By going from poly- to single-crystal waveguides, we will minimize scattering losses associated with grain boundaries (impurities decorating grains, inherent surface roughness, and grain boundary separation), and with the fabrication process (for example, stress-induced birefringence during extrusion). Our first attempts at SC fiber growth involved an inverted Czochralski method, combined with RAP chemistry to grow SC KCl fiber. In this method, molten KCl in the presence of a RAP environment is directed vertically downward through a quartz, fiber-forming orifice. To date, we have not been able to prepare any SC fiber using this apparatus because of the inability to precisely control the temperature at the liquid-solid interface. Another SC fiber growth method we have developed uses our extrusion apparatus. In this pressure-fed SC fiber growth, only a small portion of the solid is melted near the exit of the extrusion die. This forms the growth interface for fabrication of SC fibers.

The third task, optical evaluation and analysis, has been directed at understanding the nature of scattering and absorptive losses in our IR fibers. Using a scattering sphere we measured the attenuation due to scattering,  $\alpha_s$ , and the total attenuation,  $\alpha_T$ , as a function of IR laser wavelength. We found that for most fibers the scattered light varies between 40 and 60% of the total light. Further, we found that  $\alpha_T \propto \lambda^{-2}$ , and that there is no simple wavelength dependence for  $\alpha_s$ . This, we feel, is a result of scattered light being re-absorbed at the surface of the fiber. In general, our scattering measurements reveal that the surface quality of our fibers is a major source of fiber attenuation. Additional measurements of the attenuation in KRS-5 fiber while the fiber is under a constant tensile load have indicated the possibility that stress-induced birefringence may also be a major contributor to the fiber's losses. In particular, KRS-5, and very likely other ductile fiber materials (the thallium and silver halides), exhibits residual strain induced during the extrusion process. This strain and resultant variation in the index of refraction contributes to the attenuation coefficient due to scattering.

UNCLASSIFIED

SECURITY CLASSIFICATION OF THIS PAGE When Data Entered

TABLE OF CONTENTS

SECTION		Availability Codes	PAGE
1	INTRODUCTION AND SUMMARY . . . . .	Normal and/or Special	7
2	FIBER MATERIALS PREPARATION . . . . .		11
	A. Introduction . . . . .		11
	B. Approaches to be Taken . . . . .		11
	C. Experiments and Results in Materials Selection and Preparation . . . . .		12
3	FIBER FABRICATION . . . . .		19
	A. Introduction . . . . .		19
	B. Czochralski Growth of SC Fibers . . . . .		19
	C. Pressure-Fed SC Fiber Growth . . . . .		21
4	FIBER EVALUATION . . . . .		27
	A. Introduction . . . . .		27
	B. Experimental Methods . . . . .		28
	C. Transmission Spectra of KRS-5 Fiber . . . . .		31
	D. Scattering Sphere Measurements . . . . .		34
	E. Interpretation of Scattering Sphere Results . . . . .		41
	F. Stress-Induced Birefringence in Fibers . . . . .		44
	G. Experimental Set-Up and Results . . . . .		45
	H. Interpretation of Attenuation in Stressed Fibers . . . . .		49
5	FUTURE PLANS AND RECOMMENDATIONS . . . . .		51
	A. Fiber Fabrication . . . . .		51
	B. Optical Evaluation and Analysis . . . . .		53
	C. Material Considerations . . . . .		54
	PRESENTATIONS AND PAPERS . . . . .		55
	REFERENCES . . . . .		57

## LIST OF ILLUSTRATIONS

FIGURE	PAGE	
1	Projected transmission in IR fibers . . . . .	1
2	Comparative composite thermogram of (a) ALFA ultrapure thallous iodide and (b) its RAP zone refined counterpart . . . . .	15
3	Comparative composite thermogram of (a) ALFA ultrapure thallous bromide and (b) its RAP-zone-refined counterpart . . . . .	16
4	SC fiber crucible for growth and RAP purification of crystalline fibers . . . . .	22
5	Our first apparatus for inverted Czochralski growth of SC fibers . . . . .	23
6	Special die for pressure-fed, SC fiber growth . . . . .	24
7	CO <sub>2</sub> laser insertion loss apparatus . . . . .	29
8	IR fiber monochromator for 2.5 to 14.5 $\mu$ m spectral information . . . . .	30
9	Scattering measurements at IR laser wavelength . . . . .	32
10	Transmission of two KRS-5 fibers from 2.5 to 14 $\mu$ m . . . . .	33
11	Calculation of $\alpha_S$ . . . . .	35
12	Scattering losses in KRS-5 fiber at 10.6 $\mu$ m . . . . .	36
13	Effect of output end finish on $\alpha_S$ . . . . .	37
14	Scattering losses in KRS-5 fiber at two IR laser wavelengths . . . . .	39
15	Attenuation at 10.6 $\mu$ m in KRS-5 fiber with different grain size . . . . .	40
16	Percentage of scattering loss at 10.6 $\mu$ m . . . . .	42
17	Attenuation at IR laser wavelengths . . . . .	43
18	Mechanical strength of KRs-5 fiber . . . . .	46
19	Attenuation in KRS-5 fiber under applied tensile load . . . . .	47

LIST OF ILLUSTRATIONS (Continued)

FIGURE	PAGE
21      Absorption in KRS-5 fiber at 10.6 $\mu$ m while the fiber is under a constant tensile load . . . . .	47
21      Laser heating for crucible-less SC fiber growth . . . . .	52

SECTION 1  
INTRODUCTION AND SUMMARY

For the past several years, Hughes Research Laboratories has been actively engaged in the development of ultra-low-loss fiber waveguides for future long-distance communications systems. With support from contract (ONR, DARPA/NRL, and RADC) and Hughes IR&D funds, we have fabricated fibers from highly transmissive, infrared (IR) crystals. The projected losses for the alkali and thallium halides we have studied are near  $10^{-3}$  dB/km. Unfortunately, the best crystalline IR fiber made from KRS-5 (TlBrI) has a measured loss of 300 dB/km at 10.6  $\mu\text{m}$  — three orders of magnitude above the intrinsic loss for KRS-5 at this wavelength, and far above the program goal of  $10^{-3}$  dB/km.

Our approach to achieving the ultimate low-loss fiber has concentrated on developing waveguides from crystalline materials. This approach is based on theoretical predictions which show that a variety of IR crystals should have losses no greater than  $10^{-3}$  dB/km near 5  $\mu\text{m}$ .<sup>1,2</sup> For review, we show projected losses for KRS-5 and KCl in Figure 1, along with those of fused  $\text{SiO}_2$  for comparison. From these familiar V-shaped loss curves, we see that the advantage of crystalline materials derives from the shift of the multiphonon edge (Reststrahl peak) to longer wavelengths. For fused  $\text{SiO}_2$  or other oxide glasses, the multiphonon edge occurs at shorter wavelengths because of the high vibrational frequencies of the Si-O bond.

From Figure 1 we see that this limits the ultimate loss in these materials to 0.2 dB/km at 1.55  $\mu\text{m}$ , a value only recently achieved in kilometer-long lengths of silica-based fiber<sup>3</sup>. The crystalline materials, therefore, are in principle, excellent candidates for next generation waveguides if we can reduce the dominant extrinsic attenuation losses that now severely limit our crystalline fibers.

During the second year of our ONR program we have studied the purification of thallous halides and developed new methods to fabricate single crystal (SC) fibers. Combining reactive atmosphere process (RAP) chemistry techniques, which have proven so successful for alkali halides and zone refining, we have prepared thallous halide crystals for use in fiber fabrication. While we have

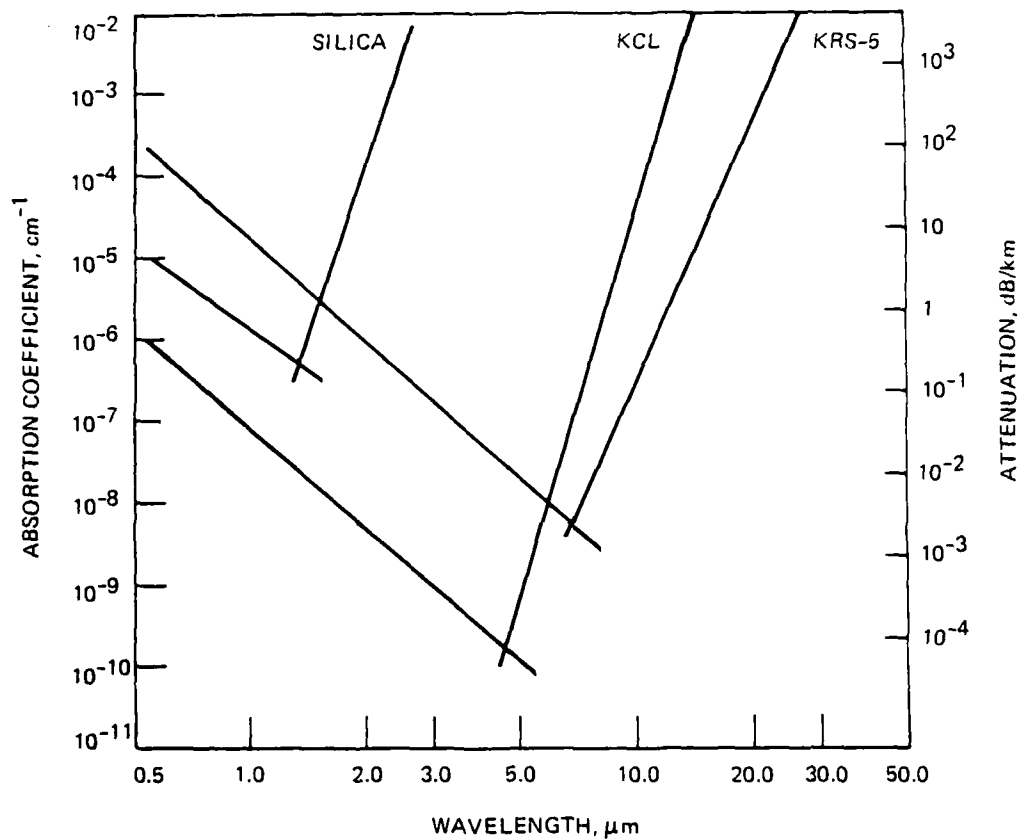


Figure 1. Projected transmission in IR fibers.

yet to evaluate these crystals optically, we expect substantial reduction in the anion impurity concentration. The fabrication of SC fibers holds, we feel, the greatest promise for achieving the program goal of  $10^{-3}$  dB/km. By going from poly to single crystal waveguides, we will minimize scattering losses associated with grain boundaries (impurities decorating grains, inherent surface roughness, and grain boundary separation), and with the fabrication process (for example, stress-induced birefringence during extrusion).

Our first attempts at SC fiber growth involved an inverted Czochralski method, combined with RAP chemistry to grow SC KCl fiber. In this method, molten KCl is directed vertically downward through a quartz, fiber-forming orifice. The melt and fiber are enclosed in an RAP atmosphere, both to purify the KCl and to reduce the surface tension between the quartz orifice and KCl fiber. To date, we have not been able to prepare any SC fiber using this apparatus because of the inability to precisely control the temperature at the liquid-solid interface. For better temperature control we have added an auxiliary heater to the apparatus.

Another SC fiber growth method we have developed used our extrusion apparatus. In this pressure-fed SC fiber growth, only a small portion of the solid is melted near the exit of the extrusion die. This forms the growth interface for fabrication of SC fibers.

In addition to fabricating IR fibers, we have been evaluating the optical and mechanical properties of the waveguides. Our optical studies have endeavored to separate scattering and absorptive losses in polycrystalline KRS-5 fibers. Using a scattering sphere we measured the attenuation due to scattering,  $\alpha_s$ , and the total attenuation,  $\alpha_T$ , as a function of IR laser wavelength. We found that for most fibers the scattered light varies between 40 and 60% of the total light. Further, we found that  $\alpha_T \propto \lambda^{-2}$ , and that there is no simple wavelength dependence for  $\alpha_s$ . This, we feel, is a result of scattered light being re-absorbed at the surface of the fiber. In general, our scattering measurements reveal that the surface quality of our fibers is a major source of fiber attenuation.

Additional measurements of the attenuation in KRS-5 fiber while the fiber is under a constant tensile load have indicated the possibility that stress-induced birefringence may also be a major contributor to the fiber's losses.

In particular, KRS-5, and very likely other ductile fiber materials (the thallium and silver halides), exhibits residual strain induced during the extrusion process. This strain and resulting variation in the index of refraction contributes to the attenuation coefficient due to scattering.

In Sections 2 through 4 we discuss the technical progress in three areas: Section 2, Fiber material preparation; Section 3, Fiber fabrication; and Section 4, Fiber evaluation. In Section 5, our recommendations for future work are given.

SECTION 2  
FIBER MATERIALS PREPARATION

A. INTRODUCTION

The fabrication of low-loss crystalline fibers requires ultra pure starting materials and new fiber fabrication techniques. In this section we describe the chemistry involved in purifying thallous halides and our attempts to prepare this material in ultra-pure form. Because we have been so successful in the extrusion of polycrystalline thallous halides, we have devoted our efforts toward preparing very pure thallous halides for use in both extrusion and single-crystal (SC) fiber growth. The primary emphasis has been on the binary, medium-melting solid solution of thallous bromide and thallous iodide, or KRS-5. The composition of this material is  $TlBr_{0.46}I_{0.54}$ .

B. APPROACHES TO BE TAKEN

In order to obtain uniformity and homogeneity in the SC fiber, crystal growth must be carried out as a steady-state operation, with the crystal growth direction along the fiber axis. Because of the relatively long crystal dimension in this direction, a fast crystal growth rate is essential; and, therefore, a melt growth method, such as the Czochralski method, the Bridgman method, or some method that is derivative of these, is much preferred over solution or flux growth methods.

To obtain fast, steady-state crystal growth from the melt, the charge material must be a congruent melter. This means that the charge material must have identical chemical compositions in its crystalline and molten phases. (In that case, no segregation or partition takes place across the crystal-to-melt interface; therefore, the compositions of the crystal and the melt are invariant during crystal growth - a necessary condition for steady-state crystal growth.) In the ideal sense, melting congruency may be interpreted to mean that the material is a pure chemical compound which is thermochemically stable in the vicinity of its melting point. In less strict and more realistic terms, it is sufficient that the concentrations of any impurities present in

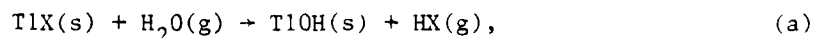
the material be below partitionable levels. We have employed the technique of zone refining under a stream of reactive gases (RAP zone refining) to raise the purity levels of commercially available thallous halides to the level of melting congruency of these materials.

There is already some evidence derived from extruded polycrystalline KRS-5 fibers that suggests that the mechanical properties of this material, namely, its yield strength, could be improved. Such improvement may be brought about by the addition of controlled quantities of specific impurities. For example, yield strength may be increased by blocking slip, which in turn may be accomplished by rendering slip planes less "smooth" through the substitution of size- or coordination-mismatched impurity species for some host ions. Dopants that may strengthen the thallous halides include  $\text{Sr}^{++}$ ,  $\text{Rb}^+$ ,  $\text{Ag}^+$ , and  $\text{Eu}^{++}$ . In the past,  $\text{Rb}^+$  and  $\text{Sr}^{++}$  have greatly strengthened the alkali halides.

#### C. EXPERIMENTS AND RESULTS IN MATERIALS SELECTION AND PREPARATION

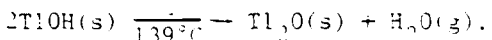
The components in KRS-5 are thallous bromide and thallous iodide; those of KRS-6 are thallous bromide and thallous chloride. The unary thallous halides were obtained by us in the form of ultrapure-grade powders from Alfa Products, Thiokol/Ventron Division. These compounds are susceptible to hydrolysis by moisture from the air, and therefore their anion purity is subject to progressive degradation even with intermittent exposure to the atmosphere.

Hydrolysis will convert the thallous halide to thallous hydroxide, as in the reaction,



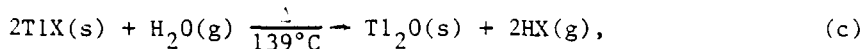
where  $\text{X}=\text{I}^-$ ,  $\text{Br}^-$ , or  $\text{Cl}^-$ . Although this reaction may be incident only on the surface of the solid, it may occur extensively in the raw materials since these are in powder form.

Thallous hydroxide readily decomposes upon heating via the reaction,



(b)

Note that the water molecule that is a product of reaction (b) may serve as a reactant in reaction (a). If the water is completely recycled, the overall reaction will be

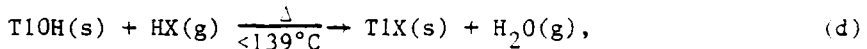


(c)

in which case each mole of water will displace two moles of halide ion. However, part of the water produced in reaction (b) is lost during calcination, and the actual extent of hydrolytic degradation will result in an  $[\text{X}^-]$  to  $[\text{H}_2\text{O}]$  ratio between one and two.\*

Thallous oxide ( $\text{Tl}_2\text{O}$ ) is a basic oxide, and has a melting point of  $300^\circ\text{C}$ , which is far below the melting points of thallous iodide, thallous bromide, or thallous chloride. (These are, respectively,  $442.5 \pm 1.0$ ,  $461.5 \pm 1.0$ , and  $431.5 \pm 1.0^\circ\text{C}$  by our own DTA measurements.) In molten form, thallous oxide will react with silica, and consequently cannot be contained by vitreous-silica ware. Indeed, our initial experiences with the "ultrapure" thallic halide powders in glass or fused-quartz containers lead us to the inevitable conclusion that these materials would have to be stripped of their hydroxide and/or oxide content before they could be melted in such containers.

The chemical stripping process that we adopted was the reversal of reaction (a) or (c), viz.,

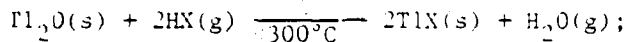


(d)

and

---

\*These anion impurities,  $\text{OH}^-$  and  $\text{O}^=$ , derived from the action of water, degrade the optical transparency of the host in the infrared. The oxygen-to-hydrogen stretch is active at  $\sim 3 \mu\text{m}$ , and the oxygen-to-metal stretch is active at  $\sim 10 \mu\text{m}$ .



e)

i.e., heating the contaminated thallous halide powder under a stream of the corresponding hydrogen halide gas without melting its thallous oxide content. Helium was used as the carrier gas so that the HX gas flow rate could be maintained at controllable levels. After approximately five hours of this treatment the thallous halide powder could be melted in vitreous-silica ware without corrosion of the latter.

Further purification of the thallous halide was carried out by RAP-zone refining with the same gas mixture. The iterative crystallization process, which is the basis of zone refining, serves to clean up the charge material via the mechanism of segregation; i.e., the expulsion from the crystal lattice of species that are alien to it. However, there are compensation reactions, either between two different alien species or between alien species and native point defects that may inhibit the segregation mechanism. In RAP-zone refining, in which a second mechanism is simultaneously provided for anion purification, many of these compensation reactions become inoperative, and the segregation mechanism is more potent.

Figures 2 and 3 show comparative DTA thermograms of pre- and post-RAP-zone-refined thallous iodide and thallous bromide, respectively. More significant than the raising of the melting point of the material by the RAP-zone-refining in both cases (2.5°C for TlI and 2.0°C for TlBr) is the sharpening of the knee of the melting endotherm, which is characteristic of melting congruency.

RAP-zone-refined thallous bromide and thallous iodide were used to grow an SC ingot of KRS-5. Its melting point was  $414.0 \pm 1.0^\circ C$  by DTA measurement. Another SC ingot of KRS-5 doped with strontium iodide to a starting concentration of 100 Sr<sup>2+</sup> ions per million cations was similarly grown. Its melting point did not deviate from that of its undoped counterpart within the limits of accuracy of the measuring procedure. There was also evidence of incomplete dissolution of the dopant.

11252-2

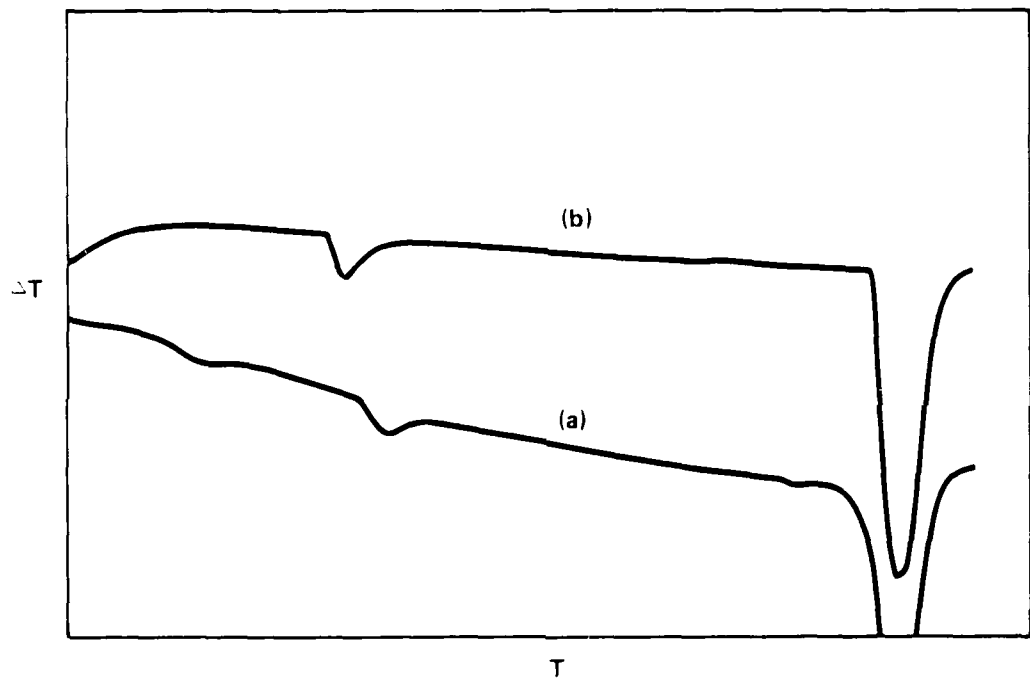


Figure 2. Comparative composite thermogram of (a) ALFA ultrapure thallous iodide and (b) its RAP zone refined counterpart. The melting point read from (a) is 440°C, and that from (b) is 442.5°C. The solid-solid transition occurs at 197.5°C in (a) and at 182.5° in (b). The shallow endotherm at around 90°C in (a), presumably the evaporation of moisture, does not appear in (b).

11252-1

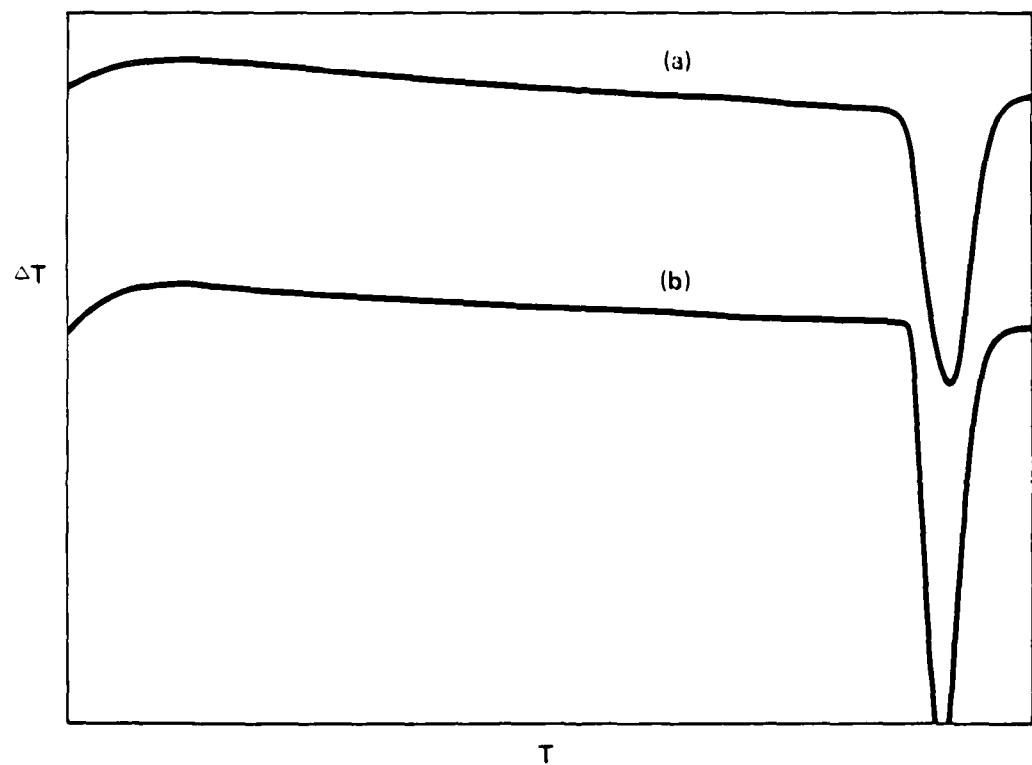


Figure 3. Comparative composite thermogram of (a) ALFA ultrapure thallous bromide and (b) its RAP-zone-refined counterpart. The melting point read from (a) is 459.5°C; that from (b) is 461.5°C.

It is expected that our zone-refining work on the thallous halides will lead to purer starting materials, and therefore lower-loss fibers. Recently, Artvushenko, et al.<sup>4</sup> at the Lebedev Russian Institute reported bulk absorption coefficients between  $3-5 \times 10^{-5} \text{ cm}^{-1}$ , or 13-11 dB/km on purified bulk KRS-5, TlCl, and KRS-6 (TlBrCl). They have indicated that  $\text{H}_2^+$  and other anion impurities such as  $\text{CO}_3^{2-}$ , and  $\text{HCO}_3^-$ , and  $\text{ClO}_3^-$  limited the bulk transmission, and that their "repeated crystallization" (probably zone-refining) improved the material. So far, we have not optically evaluated our purified materials, but we plan to do IR laser calorimetry and evaluate fibers made from these zone-refined materials during the upcoming year.

## SECTION 3

## FIBER FABRICATION

## A. INTRODUCTION

The major emphasis in fiber fabrication has been on single-crystal (SC) fiber growth. SC fibers offer significant advantages over polycrystalline fibers. Some advantages are smaller scattering losses through reduction in strain birefringence, elimination of grain boundaries, and better surface quality. During the past year we have examined the chemistry and kinetics of SC fiber growth using an inverted Czochralski growth method, and have attempted to prepare SC fibers using a modified extrusion technique.

## B. CZOCHRALSKI GROWTH OF SC FIBERS

We began our study of SC fiber growth by examining the kinetics of crystal growth for a system (fiber) which must be grown at a very uniform rate for good surface quality. The key factor in producing a uniform fiber is the surface tension of the melt. This factor will determine the kinetics of heat and mass transport at the growth interface.

The crystal growth rate,  $\dot{R}$ , based exclusively on a heat balance across the growth interface, is given by

$$\dot{R} = \frac{kM}{\rho H_c} \frac{dT}{dz} , \quad (1)$$

where  $k$  is the thermal conductivity of the crystal in the growth direction,  $M$  is its molecular weight,  $\rho$  is its density just below the melting point,  $H_c$  is its molar latent heat at crystallization, and  $dT/dz$  is the longitudinal or axial thermal gradient in the crystal just inside the growth interface. The rate of momentum transport from melt to crystal is  $\pi r^2 \rho \dot{R}^2$ . or

$$\pi r^2 \rho \dot{R}^2 = \frac{\pi r^2}{\rho} \left( \frac{kM}{H_c} \frac{dT}{dz} \right)^2 , \quad (2)$$

where  $r$  is the radius of the fiber.

The inverted Czochralski apparatus that we proposed using is shown in Figure 4. The molten halide salt is formed into fiber in the precision bore capillary. An auxiliary heater is used to obtain precise control of the growth interface. The entire system is made of quartz. In our considerations of fiber growth kinetics, the friction between the capillary may be important. Our experiments will give us empirical values for this force.

The virtual force in Equation (2) may now be included in the force-balance equation for the inverted Czochralski system. We have, for the force-balance equation,

$$\pi r^2 h \rho' g = 2\pi r \gamma + r^2 \rho R^2 \quad , \quad (3)$$

where  $h$  is the hydrostatic head of melt over the growth interface,  $\rho'$  is its density, and  $\gamma$  its surface tension. (The error in using the same  $r$  for both the melt and the crystal is negligible.) If these are indeed the only forces that come into play at the growth interface, then a comparison of the two terms on the right-hand side of the equation will yield (assuming  $r = 0.015$  cm, and  $R \approx 10$  cm/hr)

$$\frac{2\pi r \gamma}{\pi r^2 \rho R^2} \approx 10^9 \quad . \quad (4)$$

However, this equation is really incomplete in that it does not take into account the resistance to fluid flow through the capillary duct. At  $R = 10$  cm/hr, it is safe to assume viscous flow, and the Hagen-Poiseuille equation applies; i.e.,

$$\Delta p = \frac{8\mu L \dot{R}}{r^2} \quad , \quad (5)$$

where  $\Delta p$  is the pressure drop across a length,  $L$ , of duct due to resistance to flow by a fluid of viscosity,  $\mu$  (which has been estimated as equal to 1.1 cp for molten KCl from parameters tabulated in Janz' Molten Salts Handbook, Academic Press, 1967). Setting  $L/h = 1/2$ , and comparing this resistive force to the driving force (i.e., the hydrostatic force), we will obtain the ratio,

$$\frac{\pi r^2 \cdot p}{\pi r^2 h \omega g} \approx 0.0003.$$

Our initial attempts at growing SC potassium chloride fiber were carried out in a fused-quartz crucible, shown schematically in Figure 5. We used  $h = 12$  cm and  $L = 3$  cm. It eventually became apparent that control of the growth would require a closer control of the temperature of the capillary duct. To achieve this we used an auxiliary heater for this duct. This current apparatus is shown in Figure 4. Using the first inverted Czochralski apparatus for KCl fiber growth, we were unsuccessful in producing any fiber. With the better temperature control afforded by the second growth apparatus (Figure 4), we will be able to grow alkali and thallous halide fibers in next year's program.

#### C. PRESSURE-FED SC FIBER GROWTH

We have developed a new method of growing SC fibers using the extrusion apparatus normally used to fabricate polycrystalline fibers. In this method only a small portion of the crystal is melted. Figure 6 shows the special die we needed for forming SC fiber. The solid KRS-5 or TlBr (materials we have tried to date) are placed in the extrusion die body as normally done in the extrusion of polycrystalline fiber and the material is forced through the special die. In the narrow fiber-forming region of the die the crystal is melted and an SC fiber results. This method, which we call pressure-fed crystal growth, has an advantage over the first approach by having a very small melt zone, with minimal exposure to the contaminating outside environment. Furthermore, since the method used our fiber extruder, long fiber lengths are possible from the start. Finally, there is no pulling on the finished fiber. In other SC fiber techniques, the fiber is pulled by a take-up reel. This may induce strain in the fiber which can lead to scattering losses.

We have attempted a number of pressure-fed SC fiber growths using both quartz and stainless steel dies in the shape shown in Figure 6. All quartz dies cracked. We now believe this is due primarily to attack of the quartz by

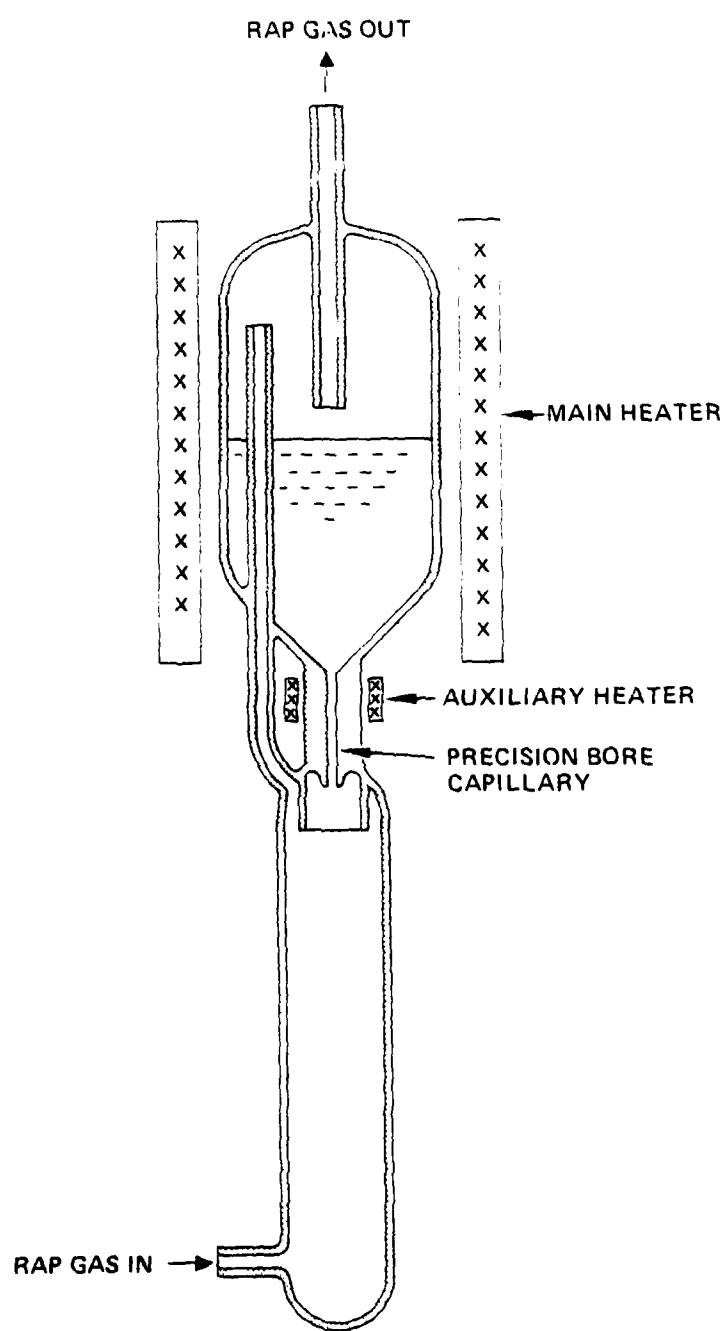


Figure 4. SC fiber crucible for growth and RAP purification of crystalline fibers.

10304-7

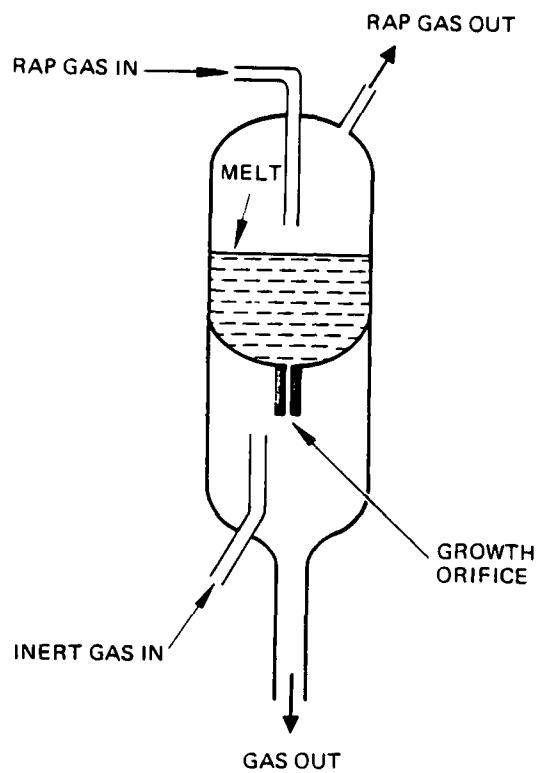


Figure 5. Our first apparatus for inverted Czochralski growth of SC fibers.

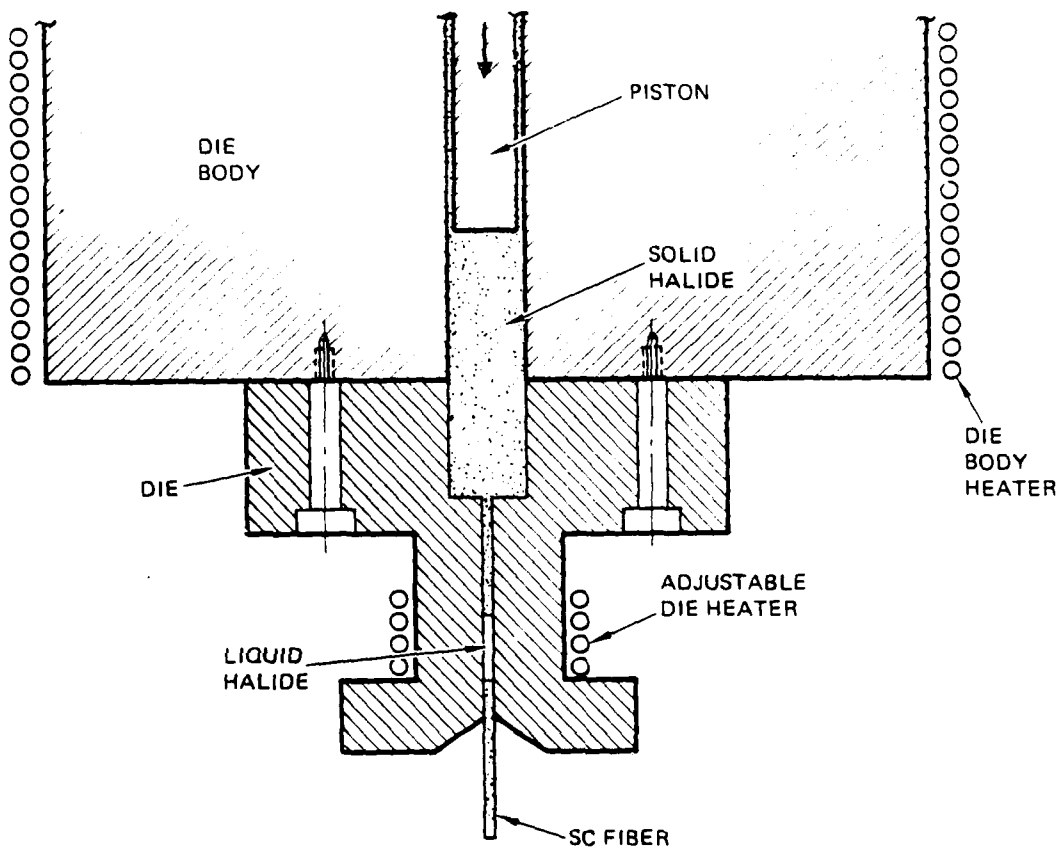


Figure 6. Special die for pressure-fed, SC fiber growth. Die is attached to die body on our extruder.

TlOH, and not the pressure placed on the die in the quasi-extrusion process. The metal die also failed during our first attempt because the melt became too hot and adhered to the metal. Future work will use other die materials, such as sapphire, to prevent interaction between the halide and the die capillary.

SECTION 4  
FIBER EVALUATION

A. INTRODUCTION

The optical evaluation of both fiber and bulk materials provides the foundation of our understanding of loss mechanisms in transparent materials. Our analysis of the optical attenuation in crystalline IR fibers has involved determining the total absorption coefficient,  $\alpha_T$ , as well as the attenuation from scattering,  $\alpha_S$ , and absorption,  $\alpha_A$ , processes. In general,

$$\alpha_T = \alpha_S + \alpha_A, \quad (6)$$

so that evaluation of  $\alpha_T$ ,  $\alpha_S$ , and  $\alpha_A$  provides a thorough understanding of the loss mechanisms in fibers.

Determination of the various attenuation coefficients can be accomplished in several different ways. In Table 1 we summarize the various experimental methods which are most commonly used. In our measurements we determined  $\alpha_T$  using both IR laser sources (insertion loss) and a small IR spectrometer of our own construction. The scattering losses were obtained using a scattering sphere. Finally,  $\alpha_A$  was obtained from  $\alpha_T$  and  $\alpha_S$  using Equation (6).

Even more information is obtained about the individual loss mechanisms if we study  $\alpha$  as a function of wavelength,  $\lambda$ . In particular, we expect a priori that  $\alpha_S$  will be a strong function of  $\lambda$  (Rayleigh scattering). Therefore, we rewrite Equation (6) to incorporate an explicit wavelength dependence:

$$\alpha_T(\lambda) = \left(\frac{A}{\lambda^4} + B\right) + \alpha_A(\lambda). \quad (7)$$

A represents Rayleigh scattering mechanisms, while B accounts for the frequency-independent scattering from particles whose size is large with respect to the wavelength. Equation (7) has been used<sup>5</sup> quite successfully to account for the observed  $\alpha_T(\lambda)$  behavior in silica-based fibers. Thus, by

TABLE I  
COMMON METHODS USED TO MEASURE ATTENUATION  
IN OPTICAL FIBERS

Attenuation Coefficient	Experimental Technique
$\alpha_T$	Insertion-loss measurement with laser IR spectroscopy
$\alpha_S$	Scattering sphere Rayleigh-Brillouin scattering
$\alpha_A$	Laser calorimetry

analogy, we anticipated that it would apply to our fibers at IR wavelengths. However, our experiments demonstrate that  $\alpha_S(\lambda)$  does not have as simple a wavelength dependence as that expressed in Equation (7).

#### B. EXPERIMENTAL METHODS

The insertion loss measurements were made at 10.6, 5.2, 3.8, and 2.8  $\mu\text{m}$  using  $\text{CO}_2$ , CO and DF/HF lasers. A diagram of the apparatus used at 10.6  $\mu\text{m}$  is shown in Figure 7. A unique feature of this set-up is the blockage of the signal reflected from the input end of the fiber. Because of the high refractive indices of our fibers, a large fraction (17% for KRS-5) is reflected at the front surface. This reflected energy can alter the laser output, creating a different incident intensity than that measured without the fiber in place. We blocked the reflected beam by using the quarter-wave plate and wire-grid polarizer, thus eliminating any enhancement of the incident energy.

Spectral information is obtained by using a broadband source (Nernst glower) and a simple monochromator. In Figure 8 we have diagrammed the essential features of our IR fiber monochromator. The wavelength selection is performed by rotating an OCL1 filter wheel (2.5 to 14.5  $\mu\text{m}$ ) at the output end of the fiber. Data are first recorded with the fiber in place, then a background or reference spectrum is recorded. The sample and reference data are established and the transmission is arbitrarily set equal to 1.0 at 10.6  $\mu\text{m}$ .

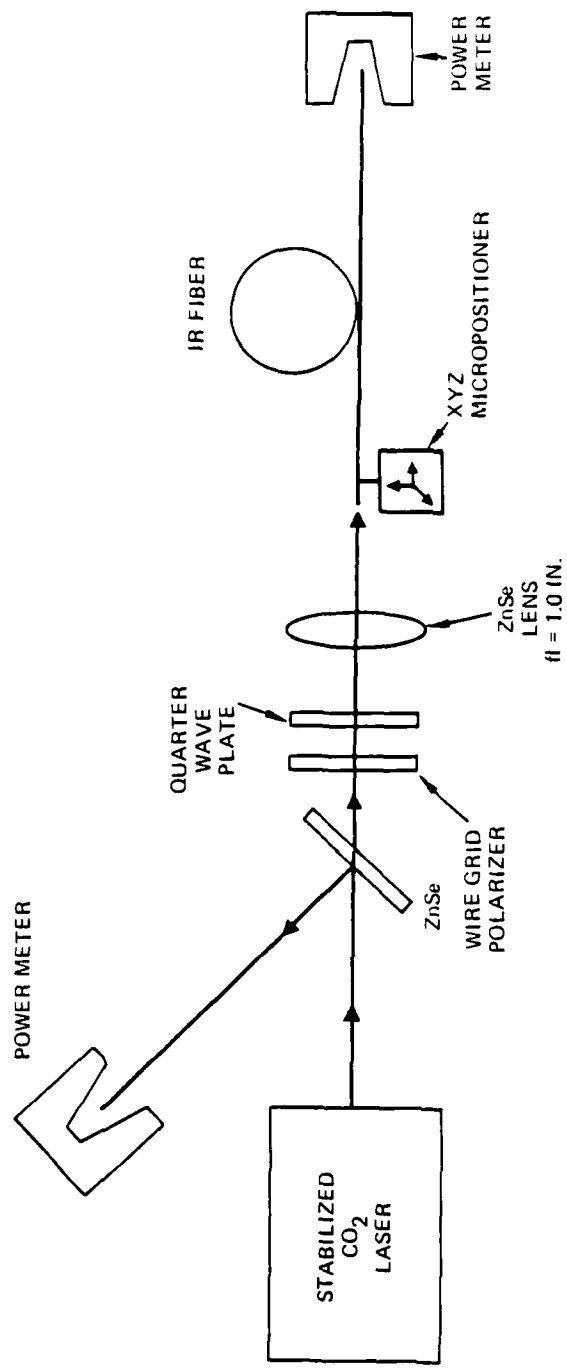


Figure 7. CO<sub>2</sub> laser insertion loss apparatus.

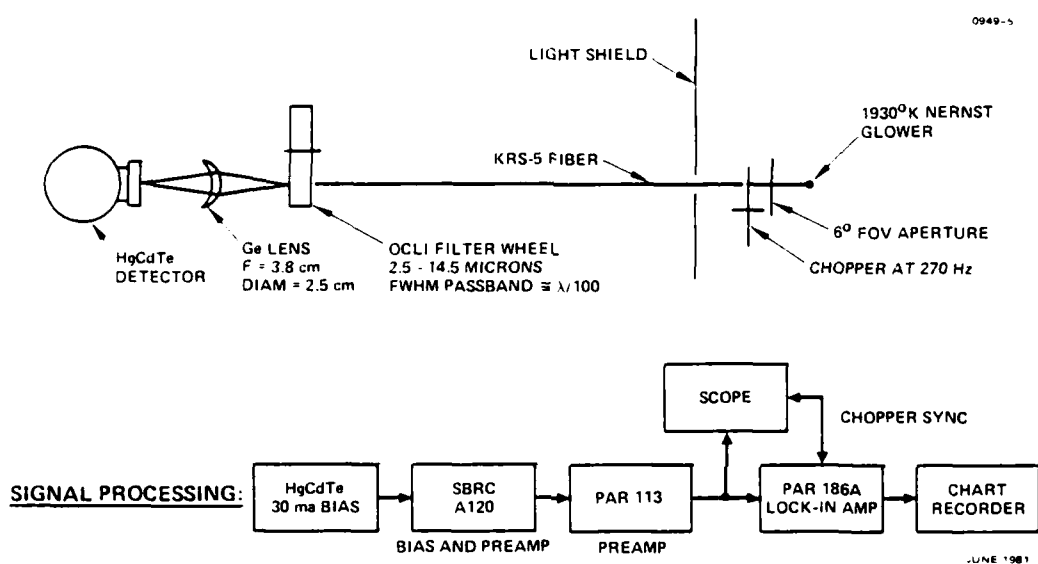
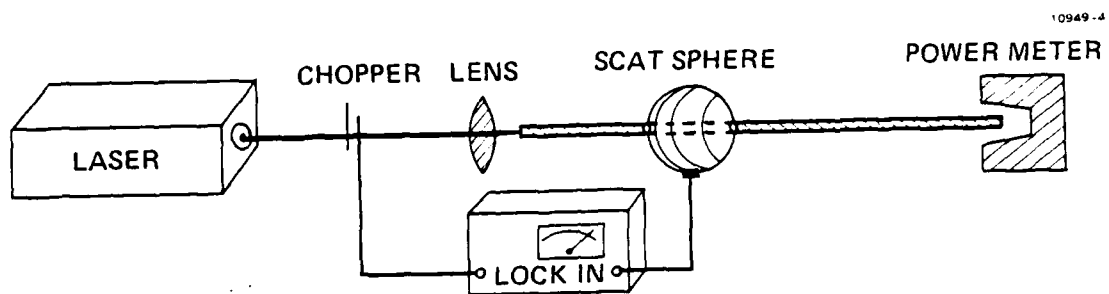


Figure 8. IR fiber monochromator for 2.5 to 14.5  $\mu\text{m}$  spectral information.

Scattering measurements were made using a small, 1.5 cm diameter scattering sphere. Scattering spheres have been used for fiber measurements on silica-glass fibers<sup>7</sup> and have been adapted for use on IR fibers.<sup>7,8</sup> The radiation scattered within the diffuse gold-coated sphere is collected by a pyroelectric detector (see Figure 9). The laser beam is chopped and phase sensitive detection is used to eliminate background radiation. The measurement is made by carefully sliding the sphere along the fiber and recording the differential scattered light as a function of position of the sphere along the fiber. The sphere and detector are calibrated at the end of the measurement by drawing the output end of the fiber into the sphere and measuring the detector signal for a known-power output of the fiber. The fibers were studied at various IR laser wavelengths (see Figure 9) to obtain our frequency dependent data.

#### C. TRANSMISSION SPECTRA OF KRS-5 FIBER

The relative transmission of two 1-m long KRS-5 fibers is given in Figure 10. The solid line shows a fiber with some impurity absorption, while the dashed line represents a fiber free of observable impurity effects. The absorption of 6.1  $\mu\text{m}$  is due to  $\text{H}_2\text{O}$ , and the 9.6  $\mu\text{m}$  band is probably due to a C-O bonded impurity. The latter band has been seen in alkali halides<sup>9</sup>, but its exact source has never been identified. In the case of the fibers we feel that the impurity absorption is on the surface of the fiber, and the fiber is acting like an ATR (attenuated total reflection) plate to reveal surface contaminants. The most striking feature of the data, however, is the decrease in transmission at the shorter wavelengths. Later, we will show that  $\tau_T \propto \lambda^{-2}$ . This behavior is characteristic of the fiber; bulk KRS-5 exhibits no decrease in transmission over this wavelength range. The most reasonable explanation for the decrease in transmission is scattering. In the next section, we will discuss the scattering measurements in greater detail and offer an explanation for the observed spectral characteristics. The transmission of the fiber (solid line in Figure 10) at IR laser wavelengths, made by insertion loss techniques, is detailed in the table in Figure 10. When these points are plotted, along with the spectral data, we see that there is good agreement between the two measurements.



<u>LASER</u>	<u>WAVELENGTH (μm)</u>
CO <sub>2</sub>	10.6
CO	5.3*
DF	3.8*
HF	2.8*

\*MULTILINE OUTPUT

Figure 9. Scattering measurements at IR laser wavelength.

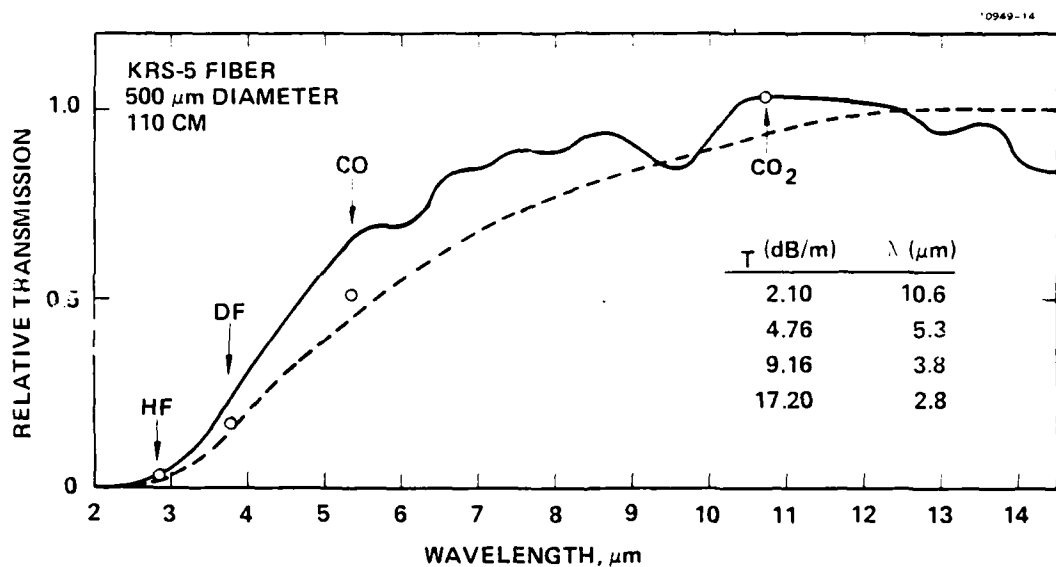


Figure 10. Transmission of two KRS-5 fibers from 2.5 to 14  $\mu\text{m}$ . Discrete joints are values of  $\alpha_T$  at IR laser wavelength.

#### D. SCATTERING SPHERE MEASUREMENTS

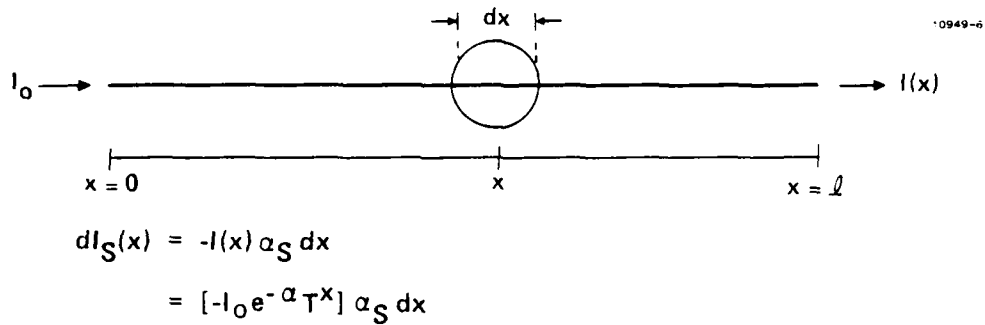
The calculation of  $\alpha_S$  has been discussed in last year's ONR contract report.<sup>7</sup> We summarize the basic relationships<sup>8</sup> needed to determine  $\alpha_S$  in Figure 11. From the defining equation for the amount of light,  $dI_S$ , scattered from a length,  $dx$ , of fiber at a distance  $x$ , from the end of the fiber,

$$dI_S = -I(x)\alpha_S dx, \quad (3)$$

from which we obtain  $\alpha_S$ . The actual value of  $\alpha_S$  depends on whether  $\alpha_S$  is obtained by integrating Equation (8) from  $x=0$  to  $x=l$  or whether  $\alpha_S$  is obtained at a few selected points using Equation (8) directly. In the first case, an average value,  $\bar{\alpha}_S$ , is obtained which includes the strong scattering contribution from the output end ( $x=l$ ) of the fiber (see Figure 12).

Differential light scattering intensity for two KRS-5 fibers is shown as a function of position along the fiber in Figure 12. In the top curve, we note the presence of a hot spot in the fiber 28 cm from the input end. The hot spot occurs where the fiber hung in the extruder overnight. At this point, the grains are large. Generally, we observe few hot spots in our present fibers, and the differential light scattering data appear as shown in the lower curve of Figure 12. Both sets of data, however, reveal excessive scattering from the output end of the fiber. This is characteristic of all our fibers and results from strong end reflections (17%) which couple light into higher order lossy modes. It is not possible to eliminate these end effects by terminating the output in an index matching fluid because there is no suitable matching liquid with a refractive index as high as that of KRS-5 ( $n=2.37$ ). Instead, we mathematically eliminate the end effect by calculating  $\alpha_S$  from Equation (8) at several points near the middle of the

The differential light scattering data of Figure 12 is used to calculate  $\alpha_S$ . For the lower curve in Figure 12 we have plotted the values,  $\alpha_S$  (calculated using Equation (8)) in Figure 13. As expected, the data show that  $\alpha_S$  is fairly constant over most of the fiber's length (note the break in abscissa in Figure 13). The solid circles are data taken on a fiber with ends polished using 0.3  $\mu\text{m}$  grit paper. This is our standard end finish for most fiber



INTEGRATION GIVES,

$$I_S(x) = \left( \frac{\alpha_S}{\alpha_T} \right) I_0 e^{-\alpha_T x}$$

OR

$$\bar{\alpha}_S = \alpha_T \left( \frac{\Delta I_S}{\Delta I_T} \right)$$

FROM DEFINITION,

$$\alpha_S = \frac{dI_S}{I_0 e^{-\alpha_T x} dx}$$

Figure 11. Calculation of  $\alpha_S$

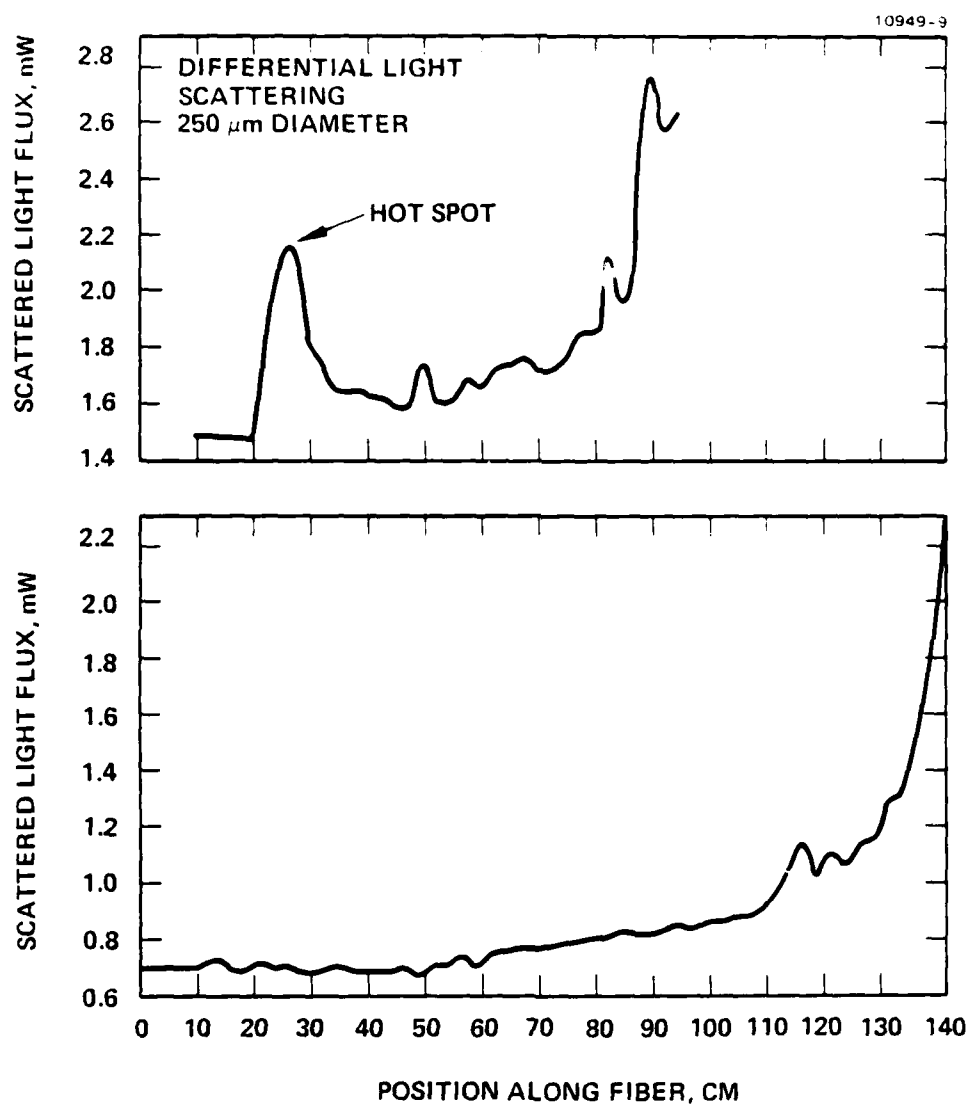


Figure 12. Scattering losses in KRS-5 fiber at 10.6  $\mu$ m.

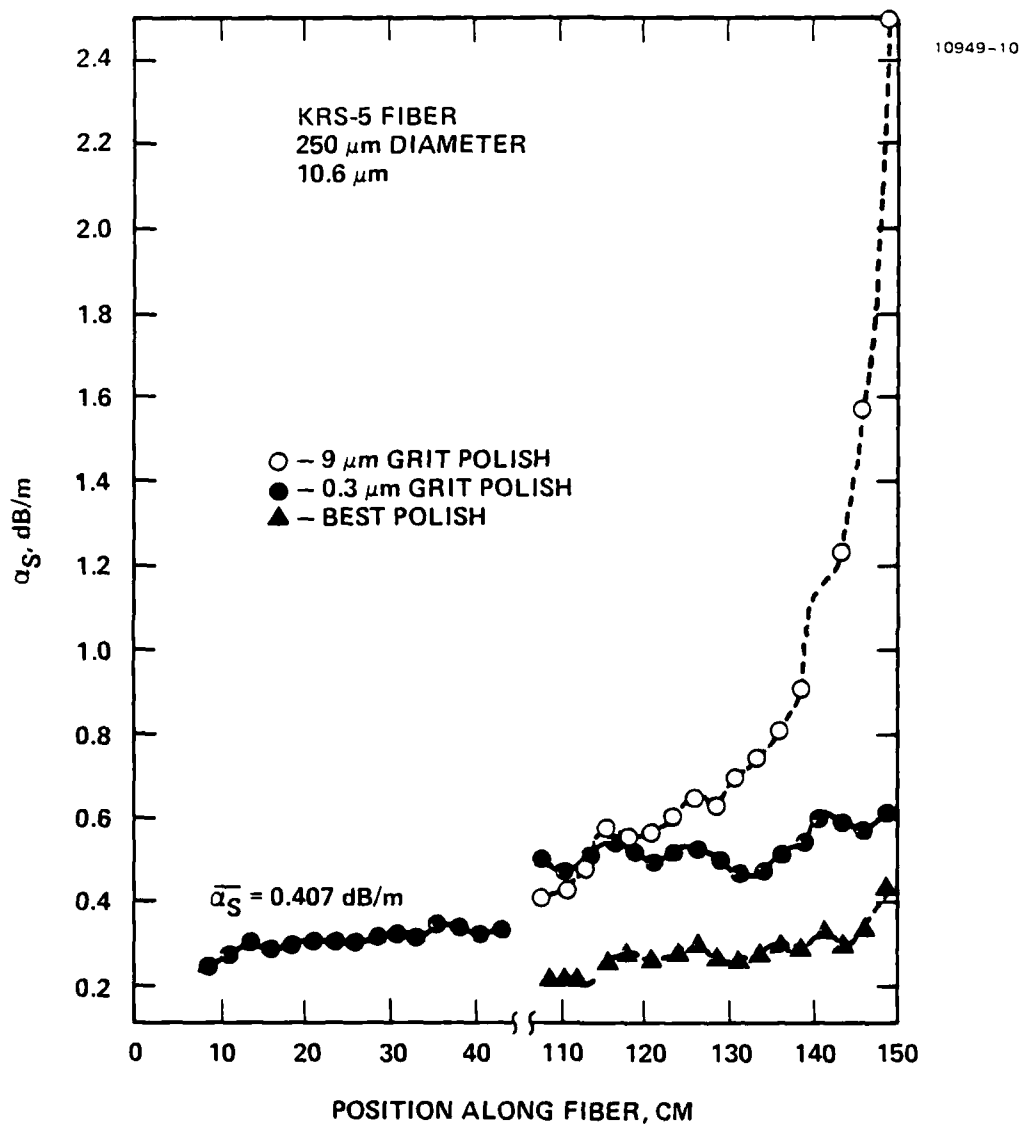


Figure 13. Effect of output end finish on  $\alpha_S$

measurements. From Figure 13 we see that the increase in  $\alpha_S$  at  $x=0$  depends on the end finish, and that the coarse grit, 9  $\mu\text{m}$  polish leads to the greatest increase in  $\alpha_S$  at the output end. The coarse end finish leads to more scattering at the end surface and thus greater losses, as expected. The best polish reduces end scattering losses to the point where there is little change in  $\alpha_S$  over the length of the fiber. We also note from Equation 13 that the average value  $\bar{\alpha}_S$  of 0.407 dB/m (includes output end scattering) for the solid-circle data is greater than the value of  $\alpha_S = 0.3$  dB/m obtained from Equation (8) and data taken near the beginning of the fiber. Therefore, we can regard  $\alpha_S = 0.3$  dB/m as more accurately representing the true scattering loss of the bulk fiber.

The effect of end scattering is even more pronounced at shorter wavelengths. Figure 14 shows data on the same fiber shown in Figure 13 with a standard end finish at two laser wavelengths. At 10.6  $\mu\text{m}$  (solid line in Figure 14),  $\alpha_S$  is observed to be relatively constant (note expanded ordinate scale as compared to Figure 13). At 5.3  $\mu\text{m}$ , however, the end scattering losses are severe, increasing almost an order of magnitude over the constant value of  $\alpha_S$ . We expected this effect at shorter wavelengths because scattering increases as the wavelength decreases.

It seems reasonable to attribute scattering losses to the polycrystalline nature of the waveguide. Specifically, the grain size would appear influential in determining the optical properties of the fiber. To check this hypothesis, we extruded two KRS-5 fibers from the same starting billet with different grain sizes. Figure 15 shows the surfaces of the 3  $\mu\text{m}$  and 34  $\mu\text{m}$  average grain size fibers, along with the measured attenuation coefficients at 10.6  $\mu\text{m}$ . We observed that even though  $\alpha_T$  varied slightly for each fiber, the ratio,  $\alpha_S/\alpha_T$ , was nearly identical for the two fibers. This means that the scattering contribution does not depend on grain size, at least within these limited test data. This is reasonable because these are cubic materials, and therefore, the random orientation of the grains by themselves should not lead to scattering losses. It is possible, however, that impurities decorating grain boundaries and inhomogeneous strain fields could lead to apparent grain size effects. At this point, we have not seen any evidence of these effects.

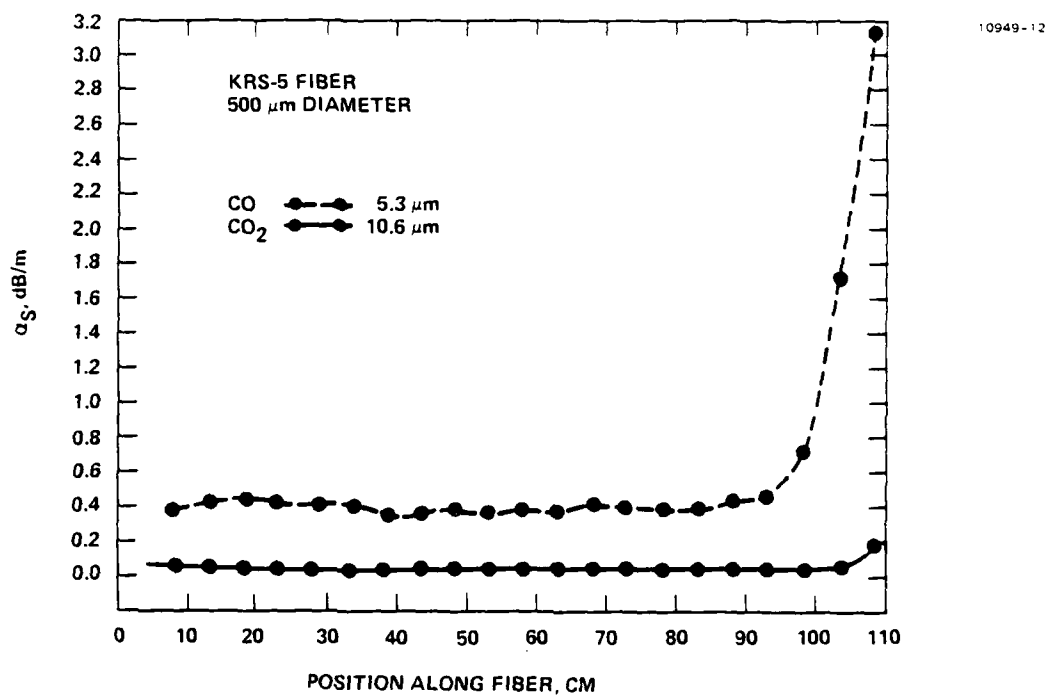


Figure 14. Scattering losses in KRS-5 fiber at two IR laser wavelengths.



1000X

AVERAGE GRAIN SIZE:  $3 \mu\text{m}$

$\bar{\alpha}_T$ (dB/m):	0.79
$\bar{\alpha}_S$ (dB/m):	0.37
$\bar{\alpha}_A$ (dB/m):	0.41
$\bar{\alpha}_S/\bar{\alpha}_T$ :	47%



1000X

$34 \mu\text{m}$

$\bar{\alpha}_T$ (dB/m):	1.14
$\bar{\alpha}_S$ (dB/m):	0.51
$\bar{\alpha}_A$ (dB/m):	0.63
$\bar{\alpha}_S/\bar{\alpha}_T$ :	45%

Figure 15. Attenuation at  $10.6 \mu\text{m}$  in KRS-5 fiber with different grain size.

We have collected all scattering measurements at 10.6  $\mu\text{m}$  to study the fraction of the total light scattered out of the fiber. The histogram in Figure 16 gives the number of fibers within a small  $\alpha_S$  range. It is evident that most fibers studied scatter between 40 to 60% of the total light. Some fibers, however, scatter only a few percent. In these cases, the total fiber loss is not reduced through the reduction of  $\alpha_S$  as might be expected. Instead,  $\alpha_T$  is as high or higher than fibers scattering 50% of the light.

Finally, the fiber attenuation data at four laser wavelengths is given in Figure 17. In the two curves,  $\alpha$  is plotted versus  $\lambda^{-1}$  to help reveal the inverse power dependence expected for  $\alpha_S$  from Equation 7. We observe from the data that for the two fibers studied,  $\alpha_T$  varies, to a good approximation, as  $\lambda^{-2}$ . However,  $\alpha_S$  does not exhibit any simple wavelength dependence. The solid lines in the  $\alpha_S$  graph show that  $\lambda^{-2}$  or  $\lambda^{-4}$  (Rayleigh scattering) do not fit the data. We must conclude that the simple frequency dependence of Equation 7 for  $\alpha_S$  does not hold for our fibers.

#### E. INTERPRETATION OF SCATTERING SPHERE RESULTS

The following two observations summarize the primary results of our attenuation measurements on KRS-5 fibers:

- The total attenuation coefficient,  $\alpha_T$ , varies as  $\lambda^{-2}$  from 2.8 to 10.6  $\mu\text{m}$ .
- The scattering attenuation coefficient,  $\alpha_S$ , is not given by  $(\frac{A}{\lambda^4} + B)$ .

At the outset, we expected that scattering and absorptive losses could be treated independently, or that  $\alpha_T = \alpha_A + \alpha_S$ . Further, we assumed  $\alpha_S$  could be broken down into a frequency dependent term which describes Rayleigh-type scattering losses, and a frequency independent term representing scattering from defects much larger than the wavelength of light. This general form of analysis has been applied to silica fibers with excellent success. Our results indicate that the situation is not so simple for our fibers. This, we feel, is due to an interaction between scattered and absorbed light which prevents us from treating each contribution separately, as described by Equation 6.

One of the major sources of attenuation is the surface quality of the fiber. Because these fibers are extruded, the surface is not as smooth as the

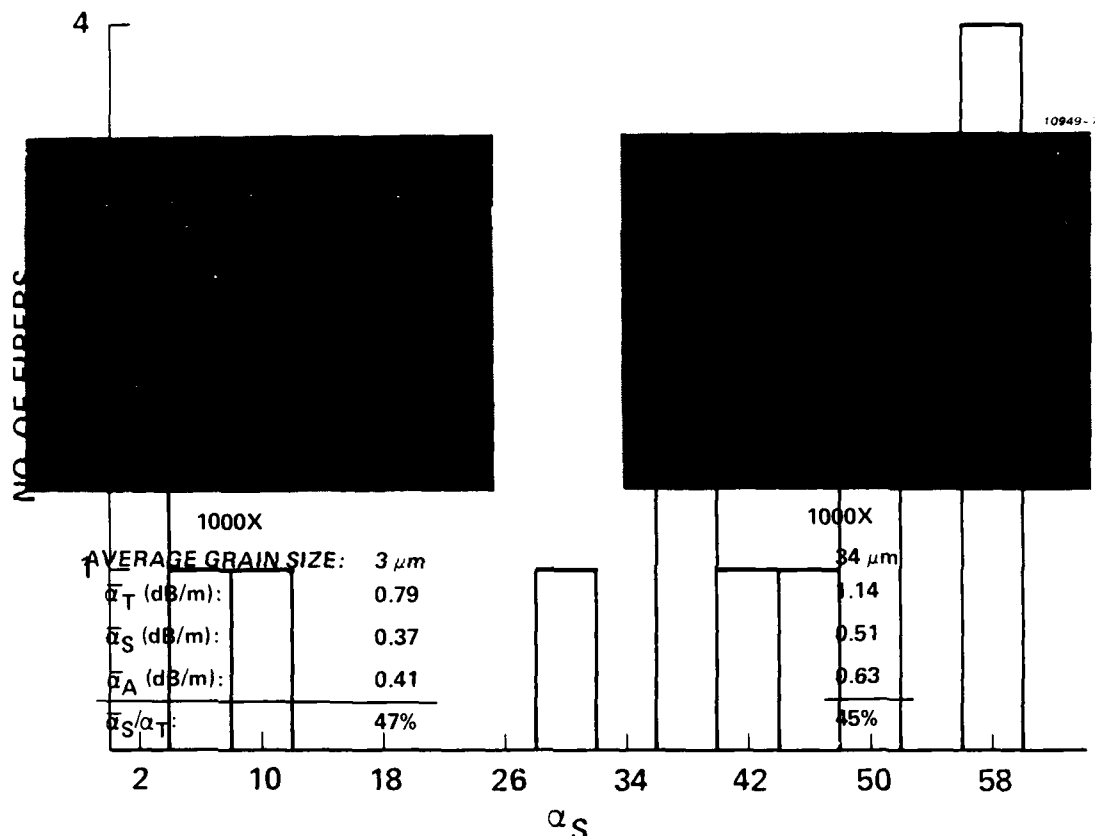


Figure 15. Attenuation  $\frac{\alpha_S}{\alpha_T} \times 100$  in KRS-5 fiber with different grain size.

Figure 16. Percentage of scattering loss at  $10.6 \mu\text{m}$ .

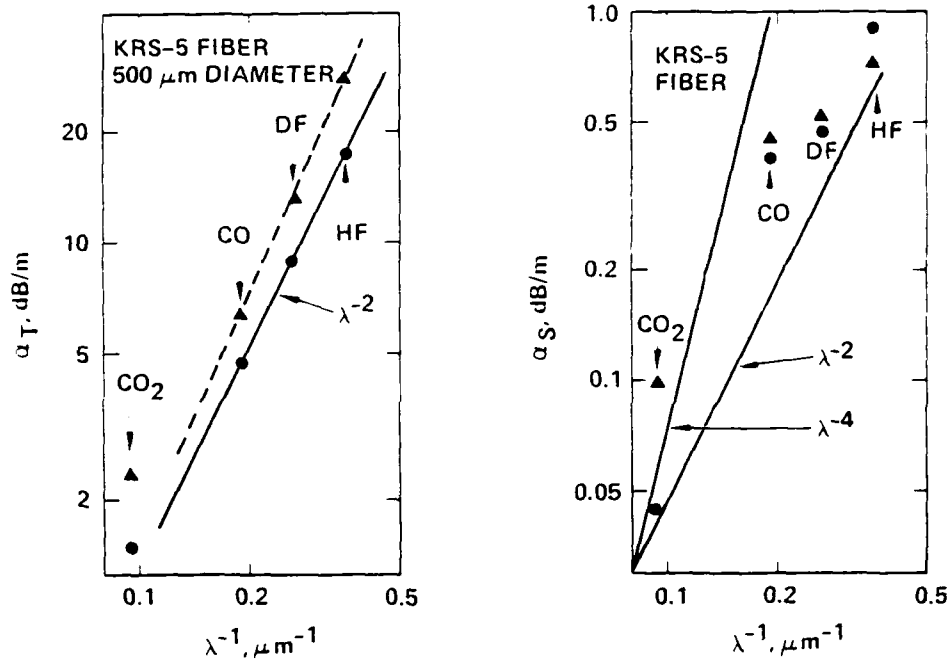


Figure 17. Attenuation at IR laser wavelengths.

free-formed surface of drawn glass fibers. The IR fiber surface is also susceptible to chemical contamination from moisture, dust, and hydrocarbons. We see the effects of such contamination in the spectral data of Figure 10. When light is scattered in the fiber from chemical defects or residual strain fields, some of the light will be scattered at angles near the critical angle (25° for KRS-5). This light will escape along the surface of the fiber and some will be absorbed by the surface. Thus, we will not collect this scattered light in our scattering sphere, and hence, this light will not properly contribute to  $\alpha_S$ . This interaction between scattering and absorption leads to an effectively smaller  $\alpha_S$ , owing to the reabsorption of scattered light. We notice this trend in the  $\alpha_S$  curve in Figure 17. We expect a strong  $\lambda^{-4}$  scattering dependence, but in fact observe a much weaker dependence of  $\alpha_S$  on  $\lambda$ , especially at the shorter wavelengths. The data show that  $\alpha_S$  does not even vary as  $\lambda^{-2}$ .

The best correlation of attenuation and wavelength is observed (see Figure 17) in the  $\alpha_T$  data. Here,  $\alpha_T$  varies as  $\lambda^{-2}$ . A  $\lambda^{-2}$ -dependence can be associated with surface absorption<sup>10</sup>; and because scattering and absorption losses are interrelated, it may seem reasonable that  $\alpha_T$  could be described by a composite  $\lambda^{-2}$ -type term. This is, however, speculative, and further analysis is necessary to properly explain the observed  $\alpha_T \sim \lambda^{-2}$  behavior.

#### F. STRESS-INDUCED BIREFRINGENCE IN FIBERS

The effect of strain on the optical properties of IR fibers is particularly important in the ductile fiber materials where the stress-induced birefringence can be significant. To determine the role of strain and its relation to the attenuation in polycrystalline KRS-5 fibers, we have undertaken a series of experiments to measure the attenuation coefficients  $\alpha_T$ ,  $\alpha_S$ , and  $\alpha_A$  as a function of applied uniaxial stress on a KRS-5 fiber. Our results indicate a strong increase in the attenuation as the fiber is loaded up to its ultimate strength.

#### G. EXPERIMENTAL SET-UP AND RESULTS

The measurements were carried out at 10.6 cm using the optical apparatus described in Section 4B. The fiber was suspended vertically and loaded with known amounts of water added to a vessel hanging from a bottom clamp. The gauge length was approximately 75 cm or 3/4 of the fiber's length. As each load was added,  $\alpha_T$  and  $\alpha_S$  were recorded. The measurements continued to the fracture point of the fiber.

A typical stress-strain curve of a KRS-5 fiber is shown in Figure 18. This curve can be used to determine the strain in our measurements, although this was not done. We note from Figure 18 the large region of plastic flow beyond the yield point. This is characteristic of these ductile polycrystalline fibers. In practice, the strain beyond yield is a function of the gauge length and loading time because this elongation is due partly to creep.

The data in Figure 19 shows the strong increase in both  $\alpha_T$  and  $\alpha_S$  as the applied load is increased. Below the yield point, the fiber loss always returns to the zero load value when the load is removed (no hysteresis). Above the yield point, the plastically deformed fiber does not return to its original loss value; instead, an extra absorption proportional to the amount of plastic deformation is added. In Figure 20 we have replotted the data in Figure 19 after subtracting the attenuation at zero load. The excess loss in Figure 20 is seen to obey a simple power law relationship with respect to applied stress.

The most likely source of the excess attenuation is stress-induced birefringence. Photomicrographs of KRS-5 fiber placed between crossed polarizers in both a relaxed and stressed state indicate considerable birefringence. This birefringence, of course, leads to scattering as a result of variations in the refractive index. M. Sparks<sup>11</sup> has recently shown that within the proportional limit fiber losses resulting from inhomogeneous strains should vary as the square of the change in refractive index,  $\Delta n$ , or

$$\alpha \sim (\Delta n)^2 \sim (q\sigma)^2, \quad (9)$$

MECHANICAL PROPERTIES

10949-2

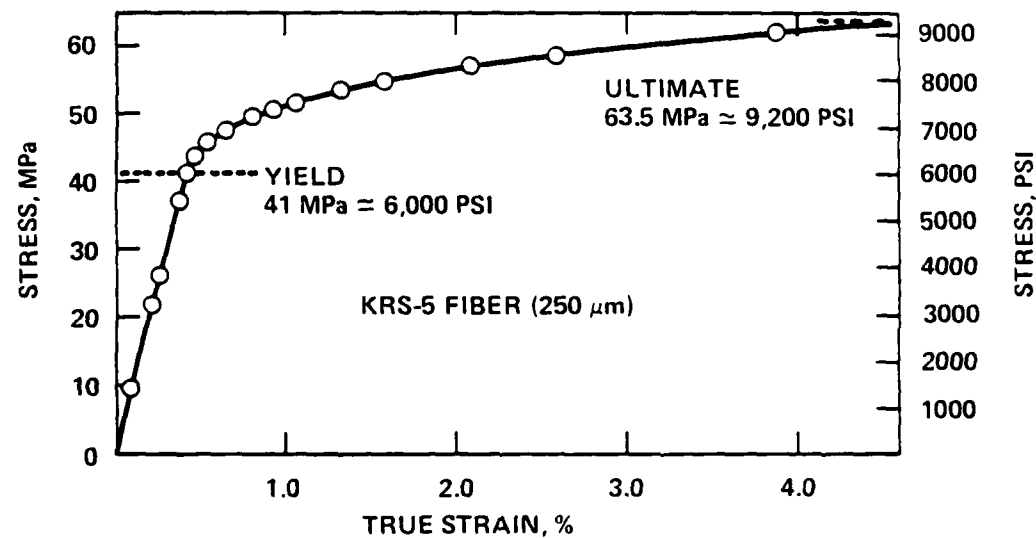


Figure 18. Mechanical strength of KRS-5 fiber.

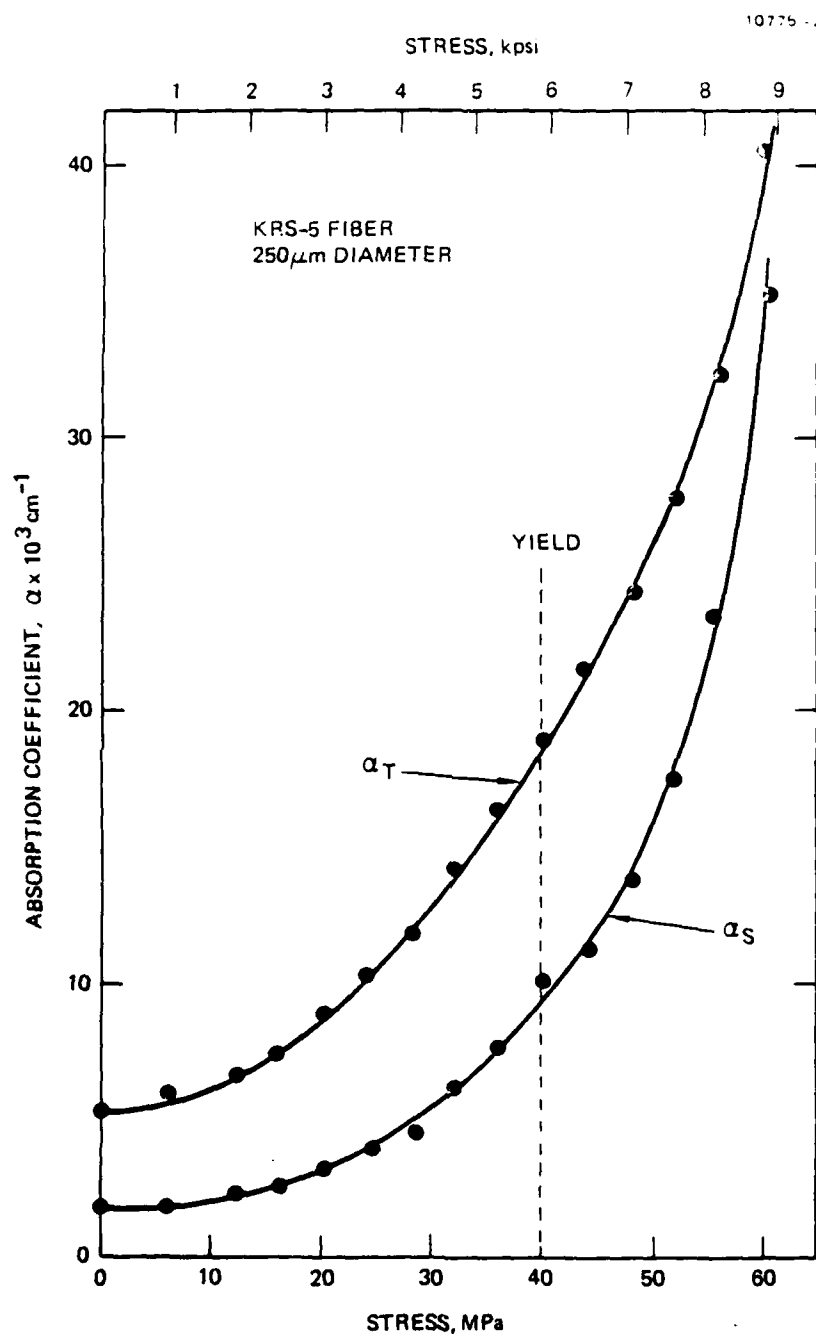


Figure 19. Attenuation in KRS-5 fiber under applied tensile load.

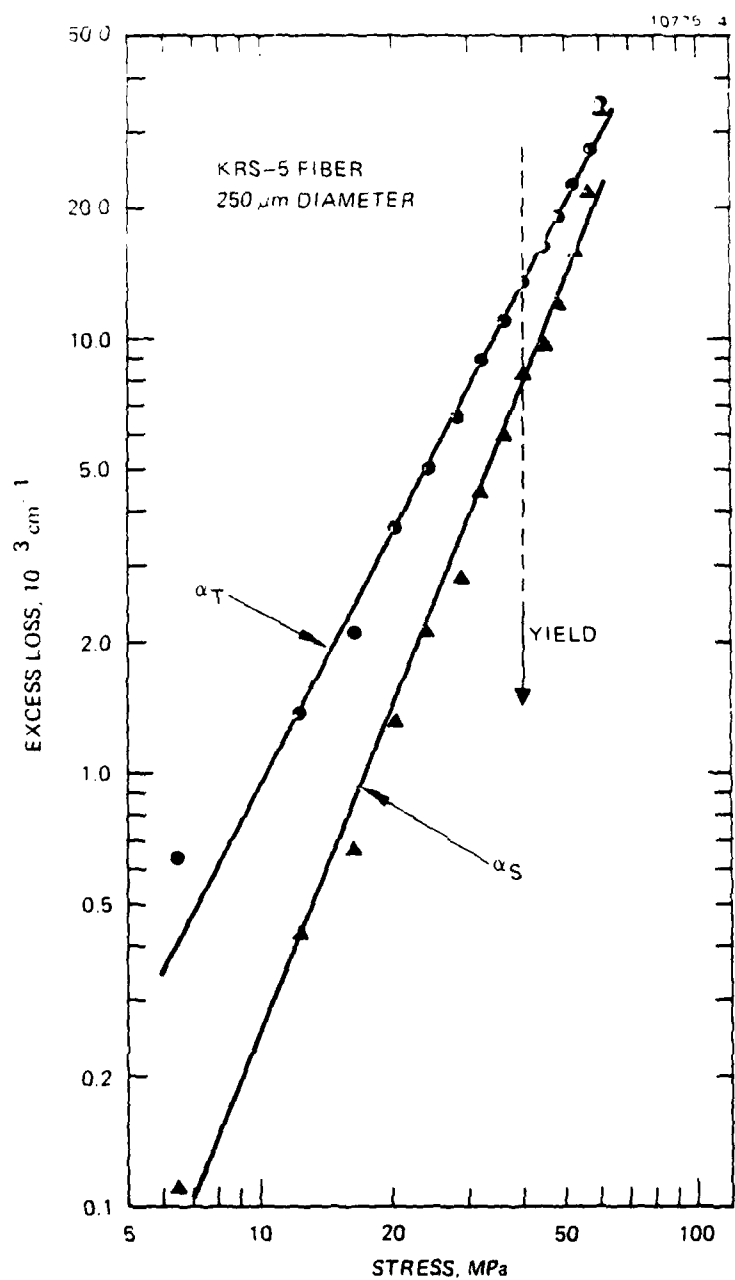


Figure 20. Absorption in KRS-5 fiber at 10.6  $\mu\text{m}$  while the fiber is under a constant tensile load. Excess loss is obtained by subtracting absorption at zero load.

where  $\sigma$  is the applied stress, and  $q$  is the stress-optic coefficient. Our results from Figure 20 show that  $\epsilon_T \approx 2.0$  and  $\epsilon_S \approx 2.5$ . This is in good agreement with Spark's calculations. Future experiments will further verify these results, especially  $\epsilon_S$ , and a more complete theory will consider the effects of voids introduced along grain boundaries and dislocations.

#### H. INTERPRETATION OF ATTENUATION IN STRESSED FIBERS

Our measurements of attenuation in stressed fibers have shown that strain birefringence is a significant loss mechanism in our fibers. The very formation of a polycrystalline fiber by extrusion induces enormous strain in the fiber. This fact, coupled with the ready deformation of these ductile materials, means that large strains will always be present in the as-extruded fiber. In fact, we now believe that, along with the surface quality, stress-induced variations in the refractive index (birefringence) may be a major source of fiber loss. In the future we will index profile the fibers to measure  $\Delta n$  directly.

The removal of strain will be difficult in our polycrystalline fibers. Annealing above 100°C will induce grain growth and weaken the waveguide. The solution seems to be single crystal fibers. SC fibers should be inherently less strained because the fabrication methods are less mechanically severe than extrusion. Further, SC fibers can be annealed to remove process-related strain.

## SECTION 5

### FUTURE PLANS AND RECOMMENDATIONS

#### A. FIBER FABRICATION

The first two years of ONR sponsored research has indicated several new directions for future work. The most important is the method of fabrication. Since the primary objective remains to develop low-loss fibers, we have decided to devote the majority of our fiber fabrication to SC fiber growth. In addition to the two approaches outlined in Section 3 to prepare SC fibers, namely, pressure-fed growth using the extruder, and the inverted Czochralski technique, we propose to add a new and novel growth method. This method is a laser initiated, crucibleless growth technique.

In this technique, laser beams are directed at the surface of the crystal to melt only a small portion of the surface of the fiber material. A seed rod (for example, a platinum wire) is dipped in the melt and a fiber is pulled vertically upward as in Czochralski growth. Figure 21 is a diagram of the concept. The advantages of this method over other SC techniques are:

- The fiber surface is not formed by any guide (such as a quartz capillary). Instead, the surface is free-formed. By analogy with glass drawing, we can expect a very smooth surface, and thus greatly reduced losses from surface roughness.
- There is less contamination of the melt by the surrounding environment because the melt is contained by its own crucible (the surrounding solid fiber material) rather than by a conventional crucible. As the melt is depleted during fiber growth, new material is melted.
- Better control of the fiber diameter is expected as opposed to conventional Czochralski growth.

Using laser heating, we may finely control the laser power to control the thermal profile. In our past experiments to seed a fiber from a KCl melt contained in a standard resistance-heated crucible we were unable to start the fiber because we could not control the temperature at the seed-liquid interface. With laser heating we have a much smaller melt region, and we expect not only easier seeding, but also good control of the fiber diameter by using an optical monitor to vary the laser power.

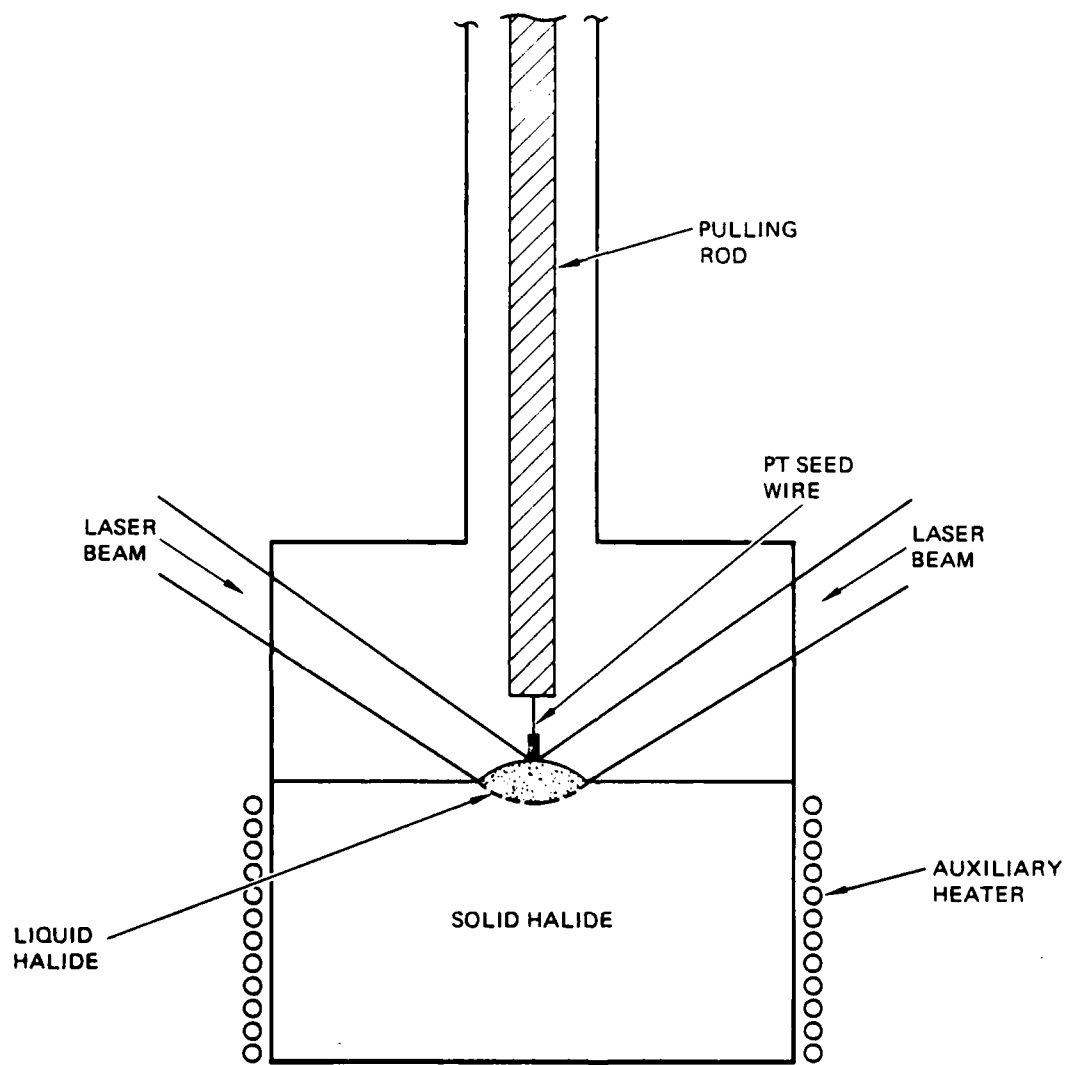


Figure 21. Laser heating for crucible-less SC fiber growth.  
Thermal expansion pushes melt up.

Our first laser heating experiments will be carried out on the thallium halides. KRS-5 and TlBr absorb strongly in the blue-green region; thus, we will use an Ar ion laser for melting. In a simple test, we required only 2 W of unfocused multiline Ar ion laser power to melt KRS-5. In the actual fiber growth experiments, we anticipate using an auxiliary resistance heater to bring the material close to the melting point (MP for KRS-5 is 410°C). The laser beams (minimum of two) would then be used to melt a small portion of the solid. We also have available a CO<sub>2</sub> laser for heating. A simple vertical pulling apparatus will be used to make the first SC fiber.

A small effort will continue in the extrusion of thallium halide fibers. These fibers allow us to study the basic loss mechanisms in IR fibers and eventually will serve as a useful comparison to the SC fibers made from the same materials. We also will be extruding some of our new purified RAP thallium halides.

#### B. OPTICAL EVALUATION AND ANALYSIS

The optical evaluation of our fibers will center on measurement of  $\alpha_T$ ,  $\alpha_S$ , and  $\alpha_A$  at infrared wavelengths. In particular, we want to study the frequency dependence of the absorption to learn more about the absorptive and scattering losses.

We will measure the index of refraction variations in our fibers by index profiling, and by evaluating the waveguides' birefringence. In the latter case, we will use a laser polariscope to obtain the average value of the birefringence across the fiber. As discussed in Section 2, we believe  $\Delta n$  may be quite large for our fibers and for most of the ductile crystalline materials in general.

We feel that a major portion of our present fiber losses are a result of surface roughness. Polycrystalline fibers are prone to a certain amount of surface roughness because of the finite grain size. We will study the effect of grain size on the fiber's attenuation by measuring,  $\alpha_T$ ,  $\alpha_S$ , and  $\alpha_A$  in fibers with different grain sizes. Grain size variation in fibers will be accomplished by thermally inducing grain growth in fibers. The surface roughness of SC fibers is expected to be substantially less than in polycrystalline fibers. However, surface irregularities may result from the SC growth

process because of the difficulty in controlling the fiber diameter. Similar absorption measurements will be made on the SC fibers, and the results will be compared to those for polycrystalline fibers.

Finally, further limited studies will be made using our Fabry-Perot Interferometer. Measurements of Rayleigh-Brillouin scattering will continue on doped and pure KCl, and scattering in the thallium halides will be initiated. These light scattering studies have helped us understand the nature of the Rayleigh scattering in bulk fiber materials. By making polarization-dependent light scattering measurements, and by evaluating the Landau-Placzek ratio,  $R_{LP}$ , as a function of temperature, we are able, in principle, to differentiate between the various elastic light scattering mechanisms. The thrust into the thallium halides will supplement our integrating sphere measurements on KRS-5 fibers, and thus help us understand the nature of our scattering losses in fibers.

#### C. MATERIAL CONSIDERATIONS

Throughout our development of low-loss IR fibers, we have emphasized the metal halides because of their potentially small residual absorption. Lately, we have focused our attention on the thallium halides, even though these crystals have not exhibited the low-loss already demonstrated for bulk alkali halides,<sup>4</sup> in particular, KCl. We feel strongly that the thallium halides afford the best near-term solution for obtaining SC fibers with losses near  $10^{-1}$  dB/km (year-end goal). One reason for this is the ease with which fibers can be made from these low melting point, ductile materials. Another is that these materials do not cleave, so that microcleavage cracks, which plagued extruded KCl fibers, will not occur in SC thallium fibers. The problem with the thallium halides is that they have not been as thoroughly studied as the alkali halides, and thus the impurity levels are greater in these materials than, for example, KCl.

PRESENTATIONS AND PAPERS

1. J. A. Harrington, M. Braunstein, B. Bobbs, and R. Braunstein, "Scattering Losses in Single and Polycrystalline Materials for Infrared Fiber Application," presented at the Physics of Fiber Optics Meeting held at the annual American Ceramic Society Meeting, 28-30 April, 1980, Chicago, Illinois. Published in *Adv. in Ceramics*, 2, *Physics of Fiber Optics*, ed. by B. Bendow and S. Mitra, p. 94, Amer. Cer. Soc., Columbus, Ohio, 1981.
2. J. A. Harrington, "Infrared Fiber Optics for CO<sub>2</sub> Laser Applications," *CO<sub>2</sub> Laser Devices and Applications*, Proc. of Soc. Photo-Opt. Instr. Eng., 227, 133-137 (1980).
3. J. A. Harrington, "A New Frontier for Optical Fibers," *Opt. Spect.*, 39-40, February, 1981.
4. J. A. Harrington, "Crystalline Infrared Fibers," *Infrared Fibers*, Proc. of Soc. Photo-Opt. Instr. Eng., 226, 10 (1981).

REFERENCES

1. M. Sparks and L. DeShazer, "Theoretical Overview of Losses in Infrared Fibers," *Infrared Fibers (0.8 - 12  $\mu$ m)*, Proc. Soc. Photo-Opt. Instr. Eng. 266, 3-9 (1981).
2. J. A. Harrington, "Crystalline Infrared Fibers," *ibid*, 10-15.
3. T. Miya, Y. Terunuma, T. Hosaka, and T. Miyashita, "Ultimate Low-Loss Single-Mode Fiber at 1.55  $\mu$ m" *Elect. Lett.*, 15, No. 4, 106-108 (1979).
4. V. G. Artyushenko, et al., "Thallium Halide Crystals with Low Optical Losses," *Sov. J. Quantum Electron.*, 10, 1181-1182 (1981).
5. D. L. Phalen and F. T. Stone, "Direct Measurement of Scattering Losses in Single-Mode and Multimode Optical Fibers," in *Advances in Ceramics, Physics of Fiber Optics*, 2, ed. by B. Bendow and S. Mitra, Amer. Cer. Soc., Columbus, Ohio, 237-245 (1981).
6. A. R. Tynes, et al., "Loss Mechanisms and Measurements in Clad Glass Fibers and Bulk Glass," *J. Opt. Soc. Amer.*, 61, 143-153 (1971).
7. J. A. Harrington, "Low-Loss Fiber Waveguides," ONR Annual Report, 1 August 1979 - 31 July 1980, Contract No. N00014-79-C-0691, Oct. 1980.
8. J. A. Harrington, "Infrared Fiber Optics for CO<sub>2</sub> Laser Applications," *CO<sub>2</sub> Laser Devices and Applications* Proc. of Soc. Photo-Opt. Instr. Eng., 227, 133-137 (1980).
9. J. M. Rowe and J. A. Harrington, "Extrinsic Absorption in KCl and KBr at CO<sub>2</sub> Laser Frequencies," *J. Appl. Phys.* 47, 4926-4928 (1976).
10. H. E. Bennett, "Scattering Characteristics of Optical Materials," *Opt. Eng.* 17, 480-488 (1978).
11. M. Sparks, "Theoretical Studies of Low-Loss Optical Fibers," Final Report, Contract No. N00173-79-C-0361, August, 1980.

ATE  
LMED  
-8